INTERNATIONAL JOURNAL FOR NUMERICAL METHODS IN FLUIDS
Int. J. Numer. Meth. Fluids 2010; **63**:584–599
Published online 9 July 2009 in Wiley InterScience (www.interscience.wiley.com). DOI: 10.1002/fld.2097

Numerical approximation of viscous terms in finite volume models for shallow waters

A. Mohammadian*, †

Department of Civil Engineering, University of Ottawa, 161 Louis Pasteur, Ottawa, ON, Canada K1N 6N5

SUMMARY

Two methods for the numerical treatment of viscous terms in shallow water equations are studied and computational details are given for structured grids. It is demonstrated that the first scheme, which is widely used, may lead to spurious oscillations arising from computational modes. In fact, the shortest resolvable waves of wave length $2\Delta x$ are invisible to this method. The second method, although more expensive, is free of computational modes and it presents a more accurate approximation of viscous terms. The dispersion relation of the second method is closer to the analytical case and it has a smaller truncation error, which is due to the fact that it uses a more localized control volume. Numerical experiments are also presented that support the study. Copyright © 2009 John Wiley & Sons, Ltd.

Received 26 February 2009; Revised 5 May 2009; Accepted 6 May 2009

KEY WORDS: shallow water; finite volume method; viscous terms; numerical errors; Fourier analysis; truncation errors; diffusion

1. INTRODUCTION

Many natural systems exhibit shallow water flow where the horizontal scales of flow are much larger than the vertical scales and the physical properties of the flow have small changes in the vertical direction compared with the horizontal ones (e.g. [1, 2]). In particular, most flows in rivers, lakes, seas and oceans are examples of shallow waters. Moreover, the shallow water equations also arise in certain atmospheric flows such as gravity waves [3].

In the past two decades, significant advances have been made in the numerical modeling of shallow water flows and many high resolution schemes have been proposed for complex flows. In

*Correspondence to: A. Mohammadian, Department of Civil Engineering, University of Ottawa, 161 Louis Pasteur, Ottawa, ON, Canada K1N 6N5.
†E-mail: majid.mohammadian@uottawa.ca

Contract/grant sponsor: Natural Sciences and Engineering Research Council of Canada (NSERC)

particular, high-order upwind finite volume schemes have become popular for hyperbolic systems due to their inherent conservation property and their ability to capture sharp gradients with a low-level of numerical diffusion and oscillations. Upwind finite volume schemes have been successfully employed for the simulation of some challenging problems for shallow flows such as dam break flows over dry and irregular topographies (e.g. [4–8]).

Fourier analysis is an approach to study the effect of discretization schemes on the properties of the continuous system. In this approach, some quantities such as wave amplitude, phase speed and group velocity are examined and the analytical form of those quantities should be preserved by an ideal numerical method. This gives us some insight into the properties of the numerical scheme and some guidelines for a proper selection of numerical parameters such as the CFL number. This approach is widely used for the study of discrete models corresponding to various equations (e.g. [9]). In particular, in the case of shallow water equations, Fourier analysis has been extensively employed for various schemes such as finite difference (e.g. [10–15]), finite element [16–21] and finite volume methods [22, 23] to examine the performance of numerical methods for various terms such as gravity and Coriolis terms.

The viscous terms in shallow water equations may become crucial in some complex flow cases including channel junctions, bend flows, and flows around hydraulic structures such as bridge piers and groynes and an accurate discretization of those terms is necessary in such cases. However, some discretization methods of viscous terms may lead to numerical noises as illustrated herein. In the present study, two commonly used numerical schemes for viscous terms are considered and a Fourier analysis as well as a detailed analysis of truncation errors and stationary modes are performed to give an insight into the performance of those schemes.

This paper is organized as follows. In Section 2 the shallow water equations are presented. Section 3 presents the finite volume method where the computational details for the treatment of convective terms and two numerical schemes for the diffusive terms are given. In Section 4, a simplified model equation for the diffusive terms is considered and the two numerical schemes for diffusive terms are studied using a Fourier analysis approach. Those results are then numerically verified in Section 5. Some concluding remarks complete the study.

2. THE SHALLOW WATER EQUATIONS

The 2-D SW equations in a conservative form may be written as

$$\frac{\partial \mathbf{u}}{\partial t}+\frac{\partial \mathbf{E}}{\partial x}+\frac{\partial \mathbf{G}}{\partial y}=\frac{\partial \mathbf{E}^{\mathrm{d}}}{\partial x}+\frac{\partial \mathbf{G}^{\mathrm{d}}}{\partial y}+\mathbf{S} \tag{1}$$

with

$$\mathbf{u}=\begin{bmatrix} h \\ u \\ v \end{bmatrix}, \quad \mathbf{E}=\begin{bmatrix} uh \\ u^2h+0.5gh^2 \\ uvh \end{bmatrix}, \quad \mathbf{G}=\begin{bmatrix} vh \\ uvh \\ v^2h+0.5gh^2 \end{bmatrix} \tag{2}$$

DOI: 10.1002/fld

where h is the water depth, u and v are the velocity components and g is the gravitational acceleration. The superscript 'd' refers to the diffusion and the corresponding flux has the following form:

$$\mathbf{E}^{\mathrm{d}}=\begin{bmatrix}0\\ \varepsilon h\dfrac{\partial u}{\partial x}\\ \varepsilon h\dfrac{\partial v}{\partial x}\end{bmatrix},\quad \mathbf{G}^{\mathrm{d}}=\begin{bmatrix}0\\ \varepsilon h\dfrac{\partial u}{\partial y}\\ \varepsilon h\dfrac{\partial v}{\partial y}\end{bmatrix} \tag{3}$$

where $\varepsilon=\nu+\nu_t$ and ν and ν_t are water and eddy viscosity coefficients, respectively. The term $\mathbf{S}$ may include various source terms such as bed roughness, Coriolis and topography. Since this paper concentrates on the viscous terms, $\mathbf{S}$ is assumed to be zero without losing generality.

3. THE FINITE VOLUME METHOD

A finite volume method is considered in this paper where all variables are located at the geometric centers of the computational cells. Let A be the area of a control volume with boundary s. The SW equations are integrated over every control volume

$$\int_t\int_A\left(\frac{\partial\mathbf{u}}{\partial x}+\frac{\partial\mathbf{E}}{\partial x}+\frac{\partial\mathbf{G}}{\partial y}-\frac{\partial\mathbf{E}^{\mathrm{d}}}{\partial x}-\frac{\partial\mathbf{G}^{\mathrm{d}}}{\partial y}\right)\mathrm{d}A\,\mathrm{d}t=0 \tag{4}$$

A high-order time-stepping scheme may be employed to integrate (4) in time. However, for the sake of simplicity and because the spatial discretization of the viscous terms is the main issue in this paper, we use the first-order forward (explicit) Euler time-stepping scheme here. This leads to

$$\int_A\left[\frac{\mathbf{u}^{n+1}-\mathbf{u}^n}{\Delta t}+\left(\frac{\partial\mathbf{E}}{\partial x}+\frac{\partial\mathbf{G}}{\partial y}-\frac{\partial\mathbf{E}^{\mathrm{d}}}{\partial x}-\frac{\partial\mathbf{G}^{\mathrm{d}}}{\partial y}\right)^n\right]\mathrm{d}A=0 \tag{5}$$

The application of the divergence theorem to the diffusive and convective flux integrals gives

$$\int_A\left(\frac{\partial\mathbf{E}}{\partial x}+\frac{\partial\mathbf{G}}{\partial y}-\frac{\partial\mathbf{E}^{\mathrm{d}}}{\partial x}-\frac{\partial\mathbf{G}^{\mathrm{d}}}{\partial y}\right)\mathrm{d}A=\oint_s(\mathbf{F}\cdot\mathbf{n}-\mathbf{F}^{\mathrm{d}}\cdot\mathbf{n})\,\mathrm{d}s \tag{6}$$

where $\mathbf{F}=(\mathbf{E},\mathbf{G})$ and $\mathbf{F}^{\mathrm{d}}=(\mathbf{E}^{\mathrm{d}},\mathbf{G}^{\mathrm{d}})$. The boundary integral is approximated by a summation over the cell interfaces (Figure 1)

$$\oint_s(\mathbf{F}\cdot\mathbf{n}-\mathbf{F}^{\mathrm{d}}\cdot\mathbf{n})\,\mathrm{d}s=\sum_{k=1}^{4}(\mathbf{F}_k\cdot\mathbf{n}_k-\mathbf{F}_k^{\mathrm{d}}\cdot\mathbf{n}_k)\,\mathrm{d}s_k \tag{7}$$

The convective flux $\mathbf{F}$ may be calculated by various schemes. Most schemes may be written in a general form as

$$\mathbf{F}=0.5(\mathbf{F}_{\mathrm{R}}+\mathbf{F}_{\mathrm{L}}-\Delta\mathbf{F}^{*}) \tag{8}$$

where $\mathbf{F}_{\mathrm{L}}=\mathbf{F}(\mathbf{u}_{\mathrm{L}})$ and $\mathbf{F}_{\mathrm{R}}=\mathbf{F}(\mathbf{u}_{\mathrm{R}})$ are the flux vectors as explained in the following. For the interfaces along the y-axis, the subscripts $._{\mathrm{R}}$ and $._{\mathrm{L}}$, respectively, represent the evaluation of the

DOI: 10.1002/fld

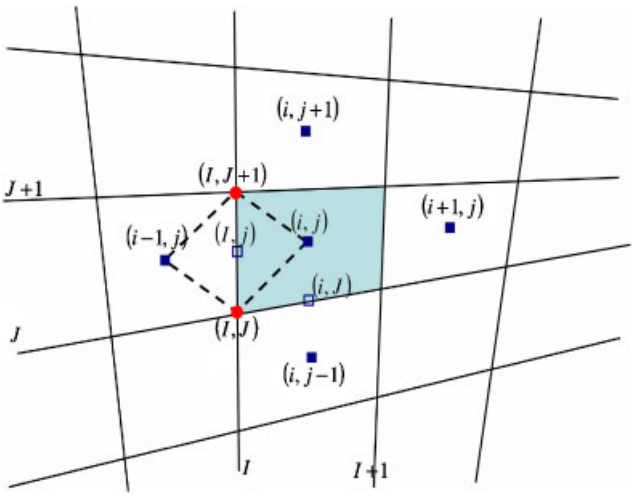

Figure 1. The cell (i, j) and its neighbors. Note that (i, j) refers to the cell center, (I, J) refers to the cell corner and (i, J) and (I, j) refer to the midpoint of the interfaces.

right and left sides of the interface, while for the interfaces along the x-axis, they respectively refer to above and below the interface. In this paper, the flux difference $\Delta\mathbf{F}^*$ is computed based on Roe's linearization,

$$\Delta\mathbf{F}^* = \sum_{k=1}^{3} \tilde{\alpha}^k |\tilde{a}^k| \tilde{\mathbf{e}}^k \tag{9}$$

where $\tilde{a}^k$, $\tilde{\mathbf{e}}^k$ and $\tilde{\alpha}^k$ are, respectively, the eigenvalues and eigenvectors of the approximate Jacobian $\tilde{\mathbf{J}}$ and the coefficients of decomposition of $\Delta\mathbf{u} = \mathbf{u}_\mathrm{R} - \mathbf{u}_\mathrm{L}$ on the basis of eigenvectors. The matrix $\tilde{\mathbf{J}}$ satisfies $\Delta\mathbf{F} = \tilde{\mathbf{J}}\Delta\mathbf{u}$ with

$$\tilde{\mathbf{J}} = \frac{\partial(\mathbf{F}\cdot\mathbf{n})}{\partial\mathbf{u}} = \begin{pmatrix} 0 & n_x & n_y \\ (\tilde{c}^2 - \tilde{u}^2)n_x - \tilde{u}\,\tilde{v}n_y & 2\tilde{u}n_x + \tilde{v}n_y & \tilde{u}n_y \\ (\tilde{c}^2 - \tilde{v}^2)n_y - \tilde{u}\,\tilde{v}n_x & \tilde{v}n_x & \tilde{u}n_x + 2\tilde{v}n_y \end{pmatrix} \tag{10}$$

where

$$\tilde{u} = \frac{u_\mathrm{R}\sqrt{h_\mathrm{R}} + u_\mathrm{L}\sqrt{h_\mathrm{L}}}{\sqrt{h_\mathrm{R}} + \sqrt{h_\mathrm{L}}}, \quad \tilde{v} = \frac{v_\mathrm{R}\sqrt{h_\mathrm{R}} + v_\mathrm{L}\sqrt{h_\mathrm{L}}}{\sqrt{h_\mathrm{R}} + \sqrt{h_\mathrm{L}}}, \quad \tilde{c} = \sqrt{\frac{g(h_\mathrm{R} + h_\mathrm{L})}{2}} \tag{11}$$

The eigenvalues of $\tilde{\mathbf{J}}$ are simply

$$\tilde{a}^1 = \tilde{u}n_x + \tilde{v}n_y + \tilde{c}, \quad \tilde{a}^2 = \tilde{u}n_x + \tilde{v}n_y, \quad \tilde{a}^3 = \tilde{u}n_x + \tilde{v}n_y - \tilde{c} \tag{12}$$

DOI: 10.1002/fld

with the corresponding eigenvectors

$$\tilde{e}^1=\begin{pmatrix}1\\ \tilde{u}+\tilde{c}n_x\\ \tilde{v}+\tilde{c}n_y\end{pmatrix},\quad \tilde{e}^2=\begin{pmatrix}1\\ -\tilde{c}n_y\\ \tilde{c}n_x\end{pmatrix},\quad \tilde{e}^3=\begin{pmatrix}1\\ \tilde{u}-\tilde{c}n_x\\ \tilde{v}-\tilde{c}n_y\end{pmatrix} \tag{13}$$

respectively. The coefficients of decomposition $\tilde{\alpha}^k$, $k=1,2,3$, are computed as

$$\tilde{\alpha}^1=\frac{\Delta h}{2}+\frac{1}{2\tilde{c}}[\Delta(hu)n_x+\Delta(hv)n_y-(\tilde{u}n_x+\tilde{v}n_y)\Delta h] \tag{14}$$

$$\tilde{\alpha}^2=\frac{1}{\tilde{c}}([\Delta(hv)-\tilde{v}\Delta h]n_x-[\Delta(hu)-\tilde{u}\Delta h]n_y) \tag{15}$$

$$\tilde{\alpha}^3=\frac{\Delta h}{2}-\frac{1}{2\tilde{c}}[\Delta(hu)n_x+\Delta(hv)n_y-(\tilde{u}n_x+\tilde{v}n_y)\Delta h] \tag{16}$$

The discretization of the diffusive terms may be performed using two approaches as explained in the following.

3.1. Method A—centered scheme for the diffusive fluxes

The diffusive fluxes in this method are approximated by a centered scheme,

$$\mathbf{F}^{\mathrm{d}}=0.5(\mathbf{F}^{\mathrm{d}}_{\mathrm{R}}+\mathbf{F}^{\mathrm{d}}_{\mathrm{L}}) \tag{17}$$

Thus, $\mathbf{E}^{\mathrm{d}}$ is computed as

$$\mathbf{E}^{\mathrm{d}}=0.5\begin{bmatrix}0\\ \left(\varepsilon h\dfrac{\partial u}{\partial x}\right)_{\mathrm{R}}+\left(\varepsilon h\dfrac{\partial u}{\partial x}\right)_{\mathrm{L}}\\ \left(\varepsilon h\dfrac{\partial v}{\partial x}\right)_{\mathrm{R}}+\left(\varepsilon h\dfrac{\partial v}{\partial x}\right)_{\mathrm{L}}\end{bmatrix} \tag{18}$$

and $\mathbf{G}^{\mathrm{d}}$ is given by

$$\mathbf{G}^{\mathrm{d}}=0.5\begin{bmatrix}0\\ \left(\varepsilon h\dfrac{\partial u}{\partial y}\right)_{\mathrm{R}}+\left(\varepsilon h\dfrac{\partial u}{\partial y}\right)_{\mathrm{L}}\\ \left(\varepsilon h\dfrac{\partial v}{\partial y}\right)_{\mathrm{R}}+\left(\varepsilon h\dfrac{\partial v}{\partial y}\right)_{\mathrm{L}}\end{bmatrix} \tag{19}$$

The interest of this approach is that in most cases, the derivatives of the velocity components are already computed at the cell centers for other purposes, such as turbulence modeling and therefore the diffusive fluxes are computed easily by a simple averaging at no extra efforts. Moreover, the general averaging (18) could be performed simultaneously with (8), which improves the computational efficiency. Note that the calculation of derivatives is straightforward in finite

DOI: 10.1002/fld

volume methods. Indeed, the divergence theorem may be employed to obtain the derivatives of a general scalar variable φ on a general cell (i, j) as (see Figure 1)

$$\left(\frac{\partial\varphi}{\partial x}\right)_{i,j} = \frac{1}{A_{i,j}}\int_A \frac{\partial\varphi}{\partial x}\,\mathrm{d}A \approx \frac{\sum_{k=1}^{4}\varphi_k\Delta y_k}{A_{i,j}} \tag{20}$$

$$\left(\frac{\partial\varphi}{\partial y}\right)_{i,j} = \frac{1}{A_{i,j}}\int_A \frac{\partial\varphi}{\partial y}\,\mathrm{d}A \approx -\frac{\sum_{k=1}^{4}\varphi_k\Delta x_k}{A_{i,j}} \tag{21}$$

where $A_{i,j}$ is the area of the control volume with vertices $(i+1, j)$, $(i, j+1)$, $(i-1, j)$ and $(i, j-1)$ and

$$\Delta x_1 = x_{i,j+1} - x_{i+1,j}, \quad \varphi_1 = (\varphi_{i,j+1} + \varphi_{i+1,j})/2 \tag{22}$$

$$\Delta x_2 = x_{i-1,j} - x_{i,j+1}, \quad \varphi_2 = (\varphi_{i-1,j} + \varphi_{i,j+1})/2 \tag{23}$$

$$\Delta x_3 = x_{i,j-1} - x_{i-1,j}, \quad \varphi_3 = (\varphi_{i,j-1} + \varphi_{i-1,j})/2 \tag{24}$$

$$\Delta x_4 = x_{i+1,j} - x_{i,j-1}, \quad \varphi_4 = (\varphi_{i+1,j} + \varphi_{i,j-1})/2 \tag{25}$$

and the computation of Δy_k is similar to Δx_k. Therefore, the viscous terms in (18) may be computed as e.g.

$$\left(\varepsilon h\frac{\partial u}{\partial x}\right)_{i,j} \approx \varepsilon h_{i,j}\frac{\sum_{k=1}^{4}u_k\Delta y_k}{A_{i,j}} \tag{26}$$

Similarly,

$$\left(\varepsilon h\frac{\partial v}{\partial y}\right)_{i,j} \approx -\varepsilon h_{i,j}\frac{\sum_{k=1}^{4}v_k\Delta x_k}{A_{i,j}} \tag{27}$$

3.2. Method B—Computation of the diffusive fluxes directly on the cell interfaces

The derivatives in this method are computed by constructing a local control volume on the cell face. The local control volume for each cell interface is defined by the center of the right and left cells and the two end points of the interface (Figure 1). Once the derivatives are obtained at the cell interfaces, the diffusive fluxes could be directly computed as $\mathbf{F}^{\mathrm{d}} = \mathbf{F}^{\mathrm{d}}_e$ where subscript $._e$ represents the values of the variables on the cell interfaces. For example, $\mathbf{E}^{\mathrm{d}}$, is computed as

$$\mathbf{E}^{\mathrm{d}} = \begin{bmatrix} 0 \\ \left(\varepsilon h\dfrac{\partial u}{\partial x}\right)_e \\ \left(\varepsilon h\dfrac{\partial v}{\partial x}\right)_e \end{bmatrix} \tag{28}$$

DOI: 10.1002/fld

The derivatives at the midpoint of a cell face e.g. (I, j) again could be computed using the divergence theorem as the method A, but now using the control volume defined by (i, j), $(I, J+1)$, $(i-1, j)$ and (I, J), i.e.

$$\begin{aligned}
&\Delta x_1 = x_{I,J+1} - x_{i,j}, \quad \varphi_1 = (\varphi_{I,J+1} + \varphi_{i,j})/2 \\
&\Delta x_2 = x_{i-1,j} - x_{I,J+1}, \quad \varphi_2 = (\varphi_{i-1,j} + \varphi_{I,J+1})/2 \\
&\Delta x_3 = x_{I,J} - x_{i-1,j}, \quad \varphi_3 = (\varphi_{I,J} + \varphi_{i-1,j})/2 \\
&\Delta x_4 = x_{i,j} - x_{I,J}, \quad \varphi_4 = (\varphi_{i,j} + \varphi_{I,J})/2
\end{aligned} \tag{29}$$

This method seems more expensive at the first glance because the values of variables at the corners of the cells are not available directly and must be obtained via an interpolation scheme. Such an interpolation step is not needed for the method A because in that method, only the value of variables at the center of control volumes is used. Therefore, the method B is computationally more expensive than the method A. However, in the next section it is shown that the method A may lead to spurious oscillations.

4. MODEL EQUATION AND FOURIER ANALYSIS

In order to give an insight into the performance of the two numerical schemes given in previous section, we consider here a two-dimensional diffusion equation in Cartesian coordinate as a model

$$\frac{\partial c}{\partial t} = \varepsilon \left(\frac{\partial^2 c}{\partial x^2} + \frac{\partial^2 c}{\partial y^2} \right) \tag{30}$$

The computation of the derivatives using the divergence theorem for a Cartesian mesh leads to

$$\begin{aligned}
\left(\frac{\partial c}{\partial x} \right)_{i,j} = 0.5[&(c_{i,j+1} + c_{i+1,j})(y_{i,j+1} - y_{i+1,j}) + (c_{i-1,j} + c_{i,j+1})(y_{i-1,j} - y_{i,j+1}) \\
&+ (c_{i,j-1} + c_{i-1,j})(y_{i,j-1} - y_{i-1,j}) + (c_{i+1,j} + c_{i,j-1})(y_{i+1,j} - y_{i,j-1})]/ \\
&[(y_{i,j+1} - y_{i,j-1})(x_{i+1,j} - x_{i-1,j})]
\end{aligned} \tag{31}$$

Thus, for a regular mesh with constant grid spacing Δx and Δy we obtain

$$\left(\frac{\partial c}{\partial x} \right)_{i,j} = \frac{c_{i+1,j} - c_{i-1,j}}{2\Delta x} \tag{32}$$

Similarly

$$\left(\frac{\partial c}{\partial y} \right)_{i,j} = \frac{c_{i,j+1} - c_{i,j-1}}{2\Delta y} \tag{33}$$

DOI: 10.1002/fld

Using the method A, the diffusive terms are approximated as

$$\left(\frac{\partial^2 c}{\partial x^2}\right)_{i,j} = \frac{0.5\left[\left(\frac{\partial c}{\partial x}\right)_{i+1,j} + \left(\frac{\partial c}{\partial x}\right)_{i,j}\right] - 0.5\left[\left(\frac{\partial c}{\partial x}\right)_{i,j} + \left(\frac{\partial c}{\partial x}\right)_{i-1,j}\right]}{\Delta x} \tag{34}$$

and

$$\left(\frac{\partial^2 c}{\partial y^2}\right)_{i,j} = \frac{0.5\left[\left(\frac{\partial c}{\partial y}\right)_{i,j+1} + \left(\frac{\partial c}{\partial y}\right)_{i,j}\right] - 0.5\left[\left(\frac{\partial c}{\partial y}\right)_{i,j} + \left(\frac{\partial c}{\partial y}\right)_{i,j-1}\right]}{\Delta y} \tag{35}$$

Computing the derivatives using (32) and (33) and substituting in (34), (35) and (30), we obtain the following equivalent of the method A:

$$\frac{\partial c}{\partial t} = \varepsilon\left(\frac{c_{i+2,j} - 2c_{i,j} + c_{i-2,j}}{4\Delta x^2} + \frac{c_{i,j+2} - 2c_{i,j} + c_{i,j-2}}{4\Delta y^2}\right) \tag{36}$$

On the other hand, with the method B, the derivatives are computed directly at the cell interfaces as

$$\begin{aligned}\left(\frac{\partial c}{\partial x}\right)_{I,j} = {} & 0.5[(c_{I,J+1} + c_{i,j})(y_{I,J+1} - y_{i,j}) + (c_{i-1,j} + c_{I,J+1})(y_{i-1,j} - y_{I,J+1}) \\ & + (c_{I,J} + c_{i-1,j})(y_{I,J} - y_{i-1,j}) + (c_{i,j} + c_{I,J})(y_{i,j} - y_{I,J})]/ \\ & [(y_{I,J+1} - y_{I,J})(x_{i,j} - x_{i-1,j})]\end{aligned} \tag{37}$$

which is simplified to

$$\left(\frac{\partial c}{\partial x}\right)_{I,j} = \frac{c_{i,j} - c_{i-1,j}}{\Delta x} \tag{38}$$

and the diffusive term is approximated as

$$\left(\frac{\partial^2 c}{\partial x^2}\right)_{i,j} = \frac{\left(\frac{\partial c}{\partial x}\right)_{I+1,j} - \left(\frac{\partial c}{\partial x}\right)_{I,j}}{\Delta x} \tag{39}$$

The term $(\partial^2 c/\partial y^2)_{i,j}$ is also computed similarly. Substituting in (30), we obtain the following equivalent of the method B:

$$\frac{\partial c}{\partial t} = \varepsilon\left(\frac{c_{i+1,j} - 2c_{i,j} + c_{i-1,j}}{\Delta x^2} + \frac{c_{i,j+1} - 2c_{i,j} + c_{i,j-1}}{\Delta y^2}\right) \tag{40}$$

First, we consider the truncation error of the two discretization approaches (36) and (40). The method A leads to

$$\varepsilon^{-1}\frac{\partial c}{\partial t} = \frac{\partial^2 c}{\partial x^2} + \frac{\partial^2 c}{\partial y^2} + \frac{\Delta x^2}{3}\frac{\partial^4 c}{\partial x^4} + \frac{\Delta y^2}{3}\frac{\partial^4 c}{\partial y^4} + \cdots \tag{41}$$

DOI: 10.1002/fld

while for the method B we obtain

$$\varepsilon^{-1}\frac{\partial c}{\partial t}=\frac{\partial^2 c}{\partial x^2}+\frac{\partial^2 c}{\partial y^2}+\frac{\Delta x^2}{12}\frac{\partial^4 c}{\partial x^4}+\frac{\Delta y^2}{12}\frac{\partial^4 c}{\partial y^4}+\cdots \tag{42}$$

which means that both methods are second-order accurate, but the method B leads to less truncation error than the method A. This could be explained by noting that, indeed, in the method B the resulting control volume for the computation of the diffusive flux is smaller. In other words, the method B uses a higher resolution than the method A in the same grid, and thus it is more accurate.

We now employ a Fourier analysis to study the solutions of the two discretization methods by comparing them with that of the continuous equation (30). Periodic solutions of (30) of the form

$$c=\tilde{c}\mathrm{e}^{\mathrm{i}(kx+ly-\omega t)} \tag{43}$$

are sought where $\tilde{c}$ is amplitude, k and l are the wave numbers in x and y directions and ω is the frequency. An equation for frequency is obtained by substituting the periodic solution in (30). This leads to the dispersion relation

$$\omega=-\mathrm{i}\varepsilon(k^2+l^2) \tag{44}$$

or

$$c=\mathrm{Re}[\tilde{c}\mathrm{e}^{\mathrm{i}(kx+ly)-\varepsilon(k^2+l^2)t}] \tag{45}$$

which means that the phase of the solution is constant and only the amplitude is damped in time and the level of the damping depends on the wave number k. Phase and group velocities are then found from their respective definitions $C:=\omega_r/k$ and $G:=\partial\omega_r/\partial k$ to be zero because the real part of the frequency (ω_r) is zero.

Dispersion relationships, phase velocities and group velocities can also be found for numerical methods by requiring nontrivial wave solutions of the discretized version of (30). An ideal numerical scheme should present similar dispersion relation to that of the continuous model (44). By substituting periodic solutions of the form $c=\tilde{c}\,\mathrm{e}^{\mathrm{i}(kx+ly-\omega t)}$ into (36) and (40), we obtain an equation for the frequency ω. The resulting dispersion relations have the following form for the two schemes:

$$-\mathrm{i}\varepsilon^{-1}\omega_{\mathrm{A}}=\frac{2\cos(2k\Delta x)-2}{4\Delta x^2}+\frac{2\cos(2l\Delta y)-2}{4\Delta y^2}\quad\text{for the method A} \tag{46}$$

$$-\mathrm{i}\varepsilon^{-1}\omega_{\mathrm{B}}=\frac{2\cos(k\Delta x)-2}{\Delta x^2}+\frac{2\cos(l\Delta y)-2}{\Delta y^2}\quad\text{for the method B} \tag{47}$$

It is observed that the frequency obtained by both schemes is pure imaginary. Hence the phase speed and group velocity are zero as for the continuous equation. Expanding the right-hand side of (46) we obtain

$$\mathrm{i}\varepsilon^{-1}\omega_{\mathrm{A}}=\frac{\sin^2(k\Delta x)}{\Delta x^2}+\frac{\sin^2(l\Delta y)}{\Delta y^2} \tag{48}$$

or

$$\varepsilon^{-1}\omega_{\mathrm{A}}=-\mathrm{i}(k^2+l^2)+\frac{\mathrm{i}k^4\Delta x^2}{3}+\frac{\mathrm{i}l^4\Delta y^2}{3}+O(\Delta x^4,\Delta y^4) \tag{49}$$

DOI: 10.1002/fld

and for the method B we obtain

$$\mathrm{i}\varepsilon^{-1}\omega_{\mathrm{A}} = \frac{2\sin^2(k\Delta x/2)}{\Delta x^2} + \frac{2\sin^2(l\Delta y/2)}{\Delta y^2} \tag{50}$$

or

$$\varepsilon^{-1}\omega_{\mathrm{B}} = -\mathrm{i}(k^2+l^2) + \frac{\mathrm{i}k^4\Delta x^2}{12} + \frac{\mathrm{i}l^4\Delta y^2}{12} + O(\Delta x^4, \Delta y^4) \tag{51}$$

That is, the dispersion relations of both discrete equations converge to that of the continuous equation with a second-order rate as Δx, $\Delta y \to 0$, but the method B has less deviation from the continuous case.

We now search for the stationary solutions of the continuous and the two discrete systems. For the continuous system, setting $\omega = 0$ in (44) leads to $k = l = 0$ and using (45), we obtain $c = \tilde{c}$. Therefore, it is observed that the continuous system only admits constant state as a stationary solution. The stationary solution for discrete system (36) is obtained by setting $\omega_{\mathrm{A}} = 0$ in (46):

$$\cos(2k\Delta x) + \cos(2l\Delta y) = 2 \tag{52}$$

or

$$k\Delta x = n\pi, \quad n = 0, 1, \ldots \tag{53}$$

$$l\Delta y = m\pi, \quad m = 0, 1, \ldots \tag{54}$$

Substituting in (43) e.g. for the case $m = n = 1$, we obtain

$$c(x_p, y_q) = \mathrm{Re}[\tilde{c}\,\mathrm{e}^{\mathrm{i}(kx_p + ly_q + \omega_{\mathrm{A}}t)}] = \tilde{c}\cos((p+q)\pi) \tag{55}$$

where $x_p = p\Delta x$ and $y_q = q\Delta y$. On the other hand, setting $\omega_{\mathrm{B}} = 0$ in (47) leads to

$$\cos(k\Delta x) + \cos(l\Delta y) = 2 \tag{56}$$

which is satisfied when

$$k\Delta x = 2n\pi, \quad n = 0, 1, \ldots \tag{57}$$

$$l\Delta y = 2m\pi, \quad m = 0, 1, \ldots \tag{58}$$

Hence, e.g., for $m = n = 1$ one obtains

$$c(x_p, y_q) = \mathrm{Re}[\tilde{c}\mathrm{e}^{\mathrm{i}(kx_p + ly_q + \omega_{\mathrm{B}}t)}] = \tilde{c}\cos(2(p+q)\pi) \tag{59}$$

A substantial difference is now observed between the solutions (55) and (59) corresponding to the two discrete systems. While the method B leads to a constant state solution as for the continuous system, the method A admits an oscillatory solution that could be potentially dangerous for the numerical simulations. Indeed, the stationary solutions of the system may be added to the unsteady solutions and still satisfy the system. Therefore, it is expected that the method B should lead to better results than the method A. A basically similar problem is also well known in the numerical modeling of the pressure terms in the Navier–Stokes equations where the first-order derivatives of pressure terms are discretized. Indeed, when velocities and water depth are co-located at the center of computational cells, numerical noises arise if a centered scheme is used for the computation

DOI: 10.1002/fld

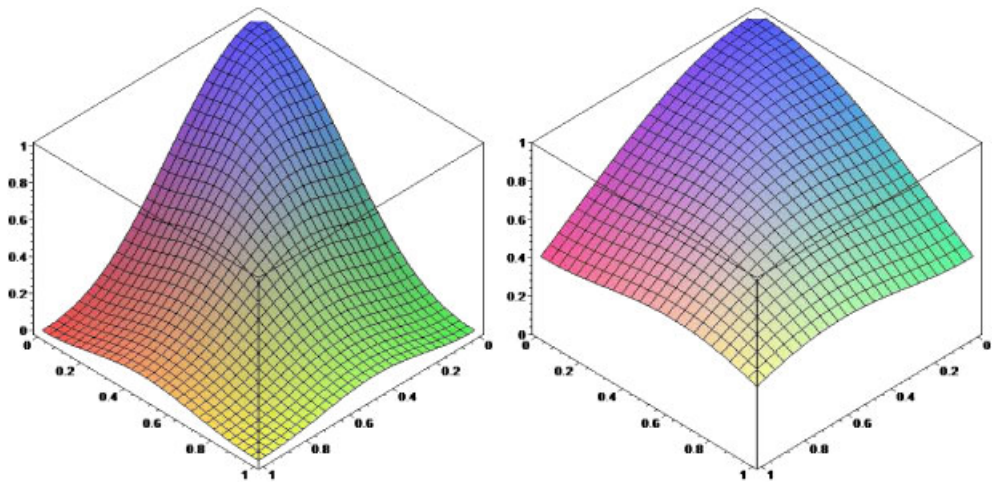

Figure 2. w_A/w (left) and w_B/w (right). The horizontal coordinates are kh/π and lh/π.

of gravity terms. This is some times called the checker board problem. However, this problem is eliminated when a flux difference splitting scheme (such as the Roe method) is used, which is the case in the present paper.

We conclude this section by plotting the ratio of discrete and continuous systems. For $\Delta x = \Delta y = h$, the ratios

$$\omega_A/\omega = \frac{2-2\cos(2kh)}{4(kh)^2+4(lh)^2)} + \frac{2-2\cos(2lh)}{4(kh)^2+4(lh)^2)} \tag{60}$$

$$\omega_B/\omega = \frac{2-2\cos(kh)}{(kh)^2+(lh)^2} + \frac{2-2\cos(lh)}{(kh)^2+(lh)^2} \tag{61}$$

are shown in Figure 2 for various wave numbers. For an ideal numerical scheme, this ratio should be equal to 1. As it is observed in Figure 2, this ratio is closer to 1 for the method B than the method A, which also shows the superiority of the method B. A comparison of the two methods for e.g. $l=0$ is shown in Figure 3. While both methods perform well for long waves, the method B leads to more accurate results for short waves than the method A. It is well known (by a discrete Fourier transform) that the wave length of the shortest resolvable waves is $2h$. As it is observed in Figure 3, the numerical frequency is zero for those waves. Thus, using the method A, the imaginary part of the numerical frequency (which corresponds to damping) is zero for the shortest resolvable waves, which means that those waves are not damped by the discretized system contrary to the behavior of the continuous system. Therefore the method A may lead to numerical oscillations. This also confirms the results obtained using analysis of stationary modes in (52).

5. NUMERICAL RESULTS

In this section three numerical experiments are performed to verify the previous results. The first case deals with the model diffusion equation (30). In this test, we show that there are stationary

DOI: 10.1002/fld

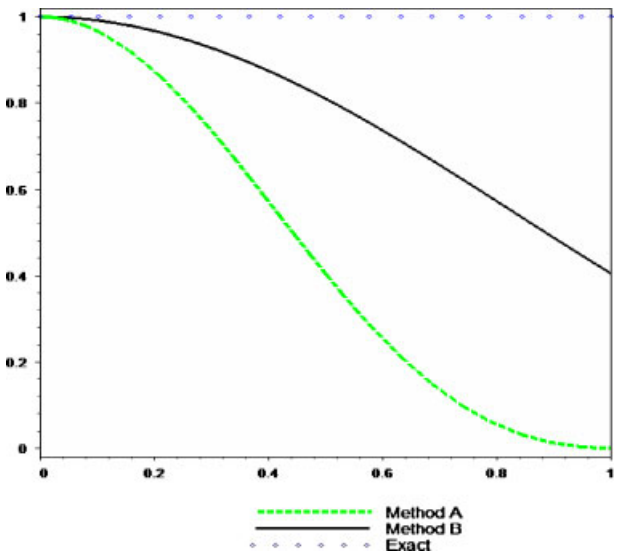

Figure 3. The ratio of frequencies w_A/w and w_B/w versus $k\Delta x/\pi$ for $l=0$.

waves that are invisible for the method A. We consider a doubly periodic $L\times L$ domain with the following initial condition:

$$c=\bar{c}\sin(2\pi x/L)\sin(2\pi y/L)+c'\cos(\pi x/\Delta x)\cos(\pi y/\Delta y) \tag{62}$$

The long wave and perturbation amplitudes are chosen as $\bar{c}=1$ and $c'=0.05$, respectively. Other employed parameters are $L=40\,\mathrm{m}$, $\varepsilon=10\,\mathrm{m}^2/\mathrm{s}$ and $\Delta x=\Delta y=1\,\mathrm{m}$. Numerical results of the methods A and B at time $t=15\,\mathrm{s}$ are shown in Figure 4. The method B has completely filtered the noise by this time, while the results of the method A are considerably noisy. The simulations were continued until steady state was obtained by both methods. In order to clearly exhibit the behavior of the two methods, initial conditions and steady-state solutions at a cross section $y=10$ are shown in Figures 5 and 6, respectively. As it is observed in Figure 6, the method B can completely damp the numerical noise and arrive at the exact solution. However, the method A can only damp the long wave, but it preserves the shortwave noise, as expected. Such a behavior could potentially lead to some oscillations in numerical simulations.

We now present an example of such noises in a shallow water model. A typical channel flow with doubly periodic boundary conditions is considered here. Initial water depth, the total viscosity ε and the domain size are assumed to be $0.2\,\mathrm{m}$, $0.005\,\mathrm{m}^2/\mathrm{s}$ and $12\times 12\,\mathrm{m}^2$, respectively. A coarse grid of size $\Delta x=\Delta y=1\,\mathrm{m}$ is employed. An initially noisy velocity field of amplitude $0.1\,\mathrm{m/s}$ is imposed as shown in Figure 7 to study the performance of the two methods in elimination of the noise. Since the width-averaged initial momentum of the flow is zero, a stagnant condition is expected as the steady-state solution (due to the effect of viscosity). Using these initial conditions, numerical simulations were performed using the methods A and B until steady-state solutions were obtained. The method B successfully eliminated the initial noise and arrived at a stagnant condition, while the method A did not change the initial noise, as expected. Indeed, those oscillations in the velocity profile are 'invisible' for the method A as discussed in the previous section.

DOI: 10.1002/fld

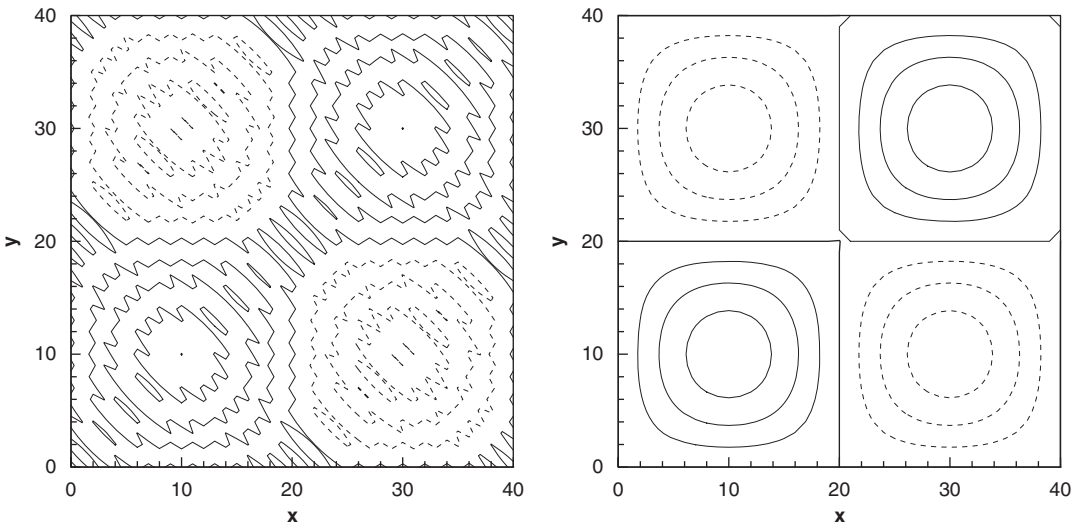

Figure 4. Results of the methods A (left) and B (right) at time $t = 15\,\mathrm{s}$.

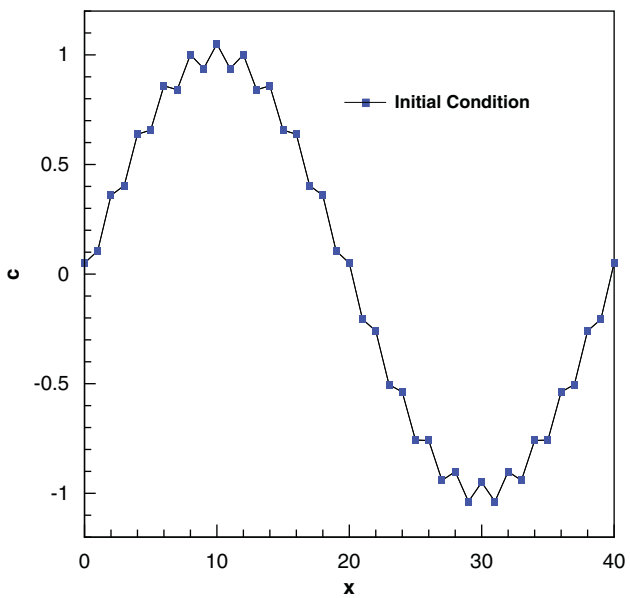

Figure 5. Initial condition at $y = 10\,\mathrm{m}$; superposition of a long and a short (noise) wave.

Finally, we consider the flow in a sudden expansion [24] as shown in Figure 8. The channel width before and after the expansion is 2 and 3 m, respectively. The water depth at the downstream and the mean inflow velocity are, respectively, 1 and 0.5 m/s. The eddy viscosity employed by Denham and Patrick is $0.00685\,\mathrm{m}^2/\mathrm{s}$ and the bottom friction is ignored. A random noisy velocity

DOI: 10.1002/fld

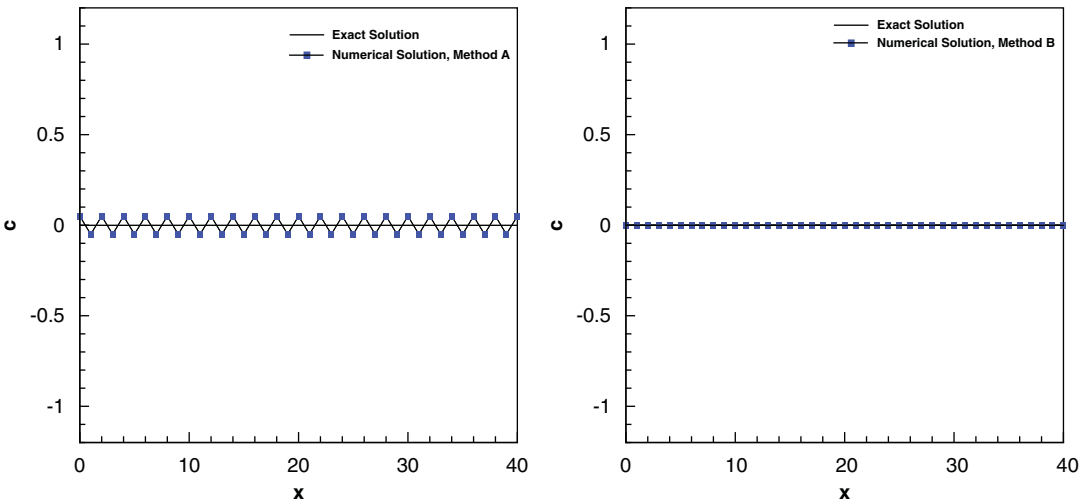

Figure 6. Steady-state solutions of the methods A (left) and B (right).

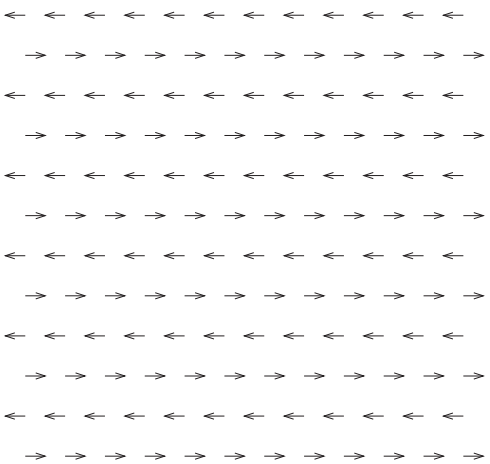

Figure 7. Initial velocity field (and steady-state solution of the method A).

field was considered as initial condition. Numerical simulation was continued until a steady-state solution was achieved. The results of the method B using a 300×100 is shown in Figure 8 where the u-component of the velocity field is compared with measured data by Denham and Patrick [24] at different sections. The method A is also able to represent roughly the same flow field at the steady state. However, it takes much longer for the method A to eliminate initial noise compared with the method B, which is again due to the numerical inaccuracy of the method A in the simulation of short waves.

DOI: 10.1002/fld

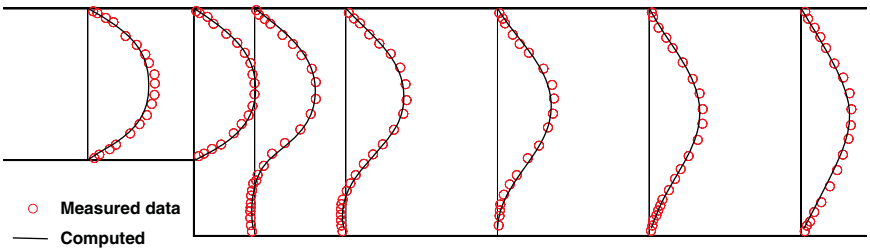

Figure 8. Flow in a sudden expansion using the method B.

6. CONCLUSION

Two numerical schemes were studied for the discretization of the viscous terms of the shallow water equations using structured grids. A Fourier analysis was performed to examine the performance of those schemes for model equations. Detailed examination of truncation errors and frequency showed that the method A may lead to spurious oscillations and large errors for short waves although it may need less computational effort. This is because the smallest resolvable waves of wavelength $2\Delta x$ are not damped by this scheme. The method B is free of those computational modes and gives more accurate results than the method A. The results are also confirmed numerically in idealized test cases.

ACKNOWLEDGEMENTS

A. Mohammadian was supported by the Natural Sciences and Engineering Research Council of Canada (NSERC).

REFERENCES

1. Vreugdenhil CB. *Numerical Methods for Shallow-water Flow*. Kluwer: Dordrecht, 1994.
2. Graf WH, Altinakar MS. *Fluvial Hydraulics*: *Flow and Transport Processes in Channels of Simple Geometry*. Wiley: England, 1998; 681. ISBN: 0-471-97714-4.
3. Marshall J, Plumb AR. *Atmosphere*, *Ocean*, *and Climate Dynamics*: *An Introductory Text*. Academic Press: New York, 2007; 319. ISBN: 0125586914, 9780125586917.
4. Mohammadian A, Le Roux D, Tajrishi M, Mazaheri K. A mass conservative scheme for simulating shallow flows over variable topography using unstructured grid. *Advances in Water Resources* 2005; **28**(5):523–537.
5. Mohammadian A, Le Roux D. Simulation of shallow flows over variable topography using unstructured grid. *International Journal for Numerical Methods in Fluids* 2006; **52**(5):473–498.
6. Zia A, Banihashemi MA. Simple efficient algorithm (SEA) for shallow flows with shock wave on dry and irregular beds. *International Journal for Numerical Methods in Fluids* 2008; **56**(11):2021–2043.
7. Noelle S, Xing Y, Shu C-W. High-order well-balanced finite volume WENO schemes for shallow water equation with moving water. *Journal of Computational Physics* 2007; **226**(1):29–58.
8. George D. Augmented Riemann solvers for the shallow water equations over variable topography with steady states and inundation. *Journal of Computational Physics* 2008; **227**(6):3089–3113.
9. Christon MA, Martinez MJ, Voth TE. Generalized Fourier analyses of the advection–diffusion equation—part I: one-dimensional domains. *International Journal for Numerical Methods in Engineering* 2004; **45**(8):839–887.
10. Batteen ML, Han YJ. On the computational noise of finite-difference schemes used in ocean models. *Tellus* 1981; **33**:387–396.
11. Wajsowicz RC. Free planetary waves in finite-difference numerical models. *Journal of Physical Oceanography* 1986; **16**:773–789.

DOI: 10.1002/fld

12. Neta B, Williams RT. Rossby wave frequencies and group velocities for finite element and finite difference approximations to the vorticity-divergence and the primitive forms of the shallow water equations. *Monthly Weather Review* 1989; **117**:1439–1457.
13. Randall DA. Geostrophic adjustment and the finite-difference shallow-water equations. *Monthly Weather Review* 1994; **122**:1371–1377.
14. Adcroft AJ, Hill CN, Marshall JC. A new treatment of the Coriolis terms in C-grid models at both high and low resolutions. *Monthly Weather Review* 1999; **127**(8):1928–1936.
15. Sankaranarayanan S, Spaulding ML. Dispersion and stability analyses of the linearized two-dimensional shallow water equations in boundary-fitted co-ordinates. *International Journal for Numerical Methods in Engineering* 2003; **42**(7):741–763.
16. Foreman MGG. An analysis of the wave equation model for finite element tidal computations. *Journal of Computational Physics* 1983; **52**:290–312.
17. Walters R, Carey GF. Numerical noise in ocean and estuarine models. *Advances in Water Resources* 1984; **7**(1):15–20.
18. Le Roux DY, Carey GF. Dispersion analysis of the least-squares finite-element shallow-water system. *International Journal for Numerical Methods in Fluids* 2003; **42**(6):607–622.
19. Le Roux DY, Carey GF. Stability/dispersion analysis of the discontinuous Galerkin linearized shallow-water system. *International Journal for Numerical Methods in Fluids* 2005; **48**(3):325–347.
20. Le Roux DY, Rostand V, Pouliot B. Analysis of numerically-induced oscillations in 2D finite-element shallow-water models—part I: inertia–gravity waves. *SIAM Journal on Scientific Computing* 2007; **29**:331–360.
21. Le Roux DY, Pouliot B. Analysis of numerically-induced oscillations in two-dimensional finite-element shallow-water models—part II: free planetary waves. *SIAM Journal on Scientific Computing* 2008; **30**:1971–1991.
22. Szpilka CM, Kolar RL. Numerical analogs of Fourier and dispersion analysis: development, verification, and application to the shallow water equations. *Advances in Water Resources* 2003; **26**:649–662.
23. Mohammadian A, Le Roux D. Fourier analysis of a class of upwind schemes in shallow water systems for gravity and Rossby waves. *International Journal for Numerical Methods in Fluids* 2008; **57**(4):389–416.
24. Denham MK, Patrick MA. Laminar flow over a downstreamfacing step in a two-dimensional flow channel. *Transactions of the Institution of Chemical Engineers* 1974; **52**:361.

DOI: 10.1002/fld